Agricultural and Forest Meteorology 214-215 (2015) 189–200

Contents lists available at ScienceDirect

Agricultural and Forest Meteorology

journal homepage: www.elsevier.com/locate/agrformet

Impacts of soil heat flux calculation methods on the surface energy balance closure

Eric S. Russell [a], Heping Liu [a,*], Zhongming Gao [a], Dennis Finn [b], Brian Lamb [a]

[a] Laboratory for Atmospheric Research, Department of Civil and Environmental Engineering, Washington State University, Pullman, WA 99164, USA
[b] NOAA/Air Resources Laboratory Field Research Division, Idaho Falls, ID, USA

ARTICLE INFO

Article history:
Received 24 February 2015
Received in revised form 17 July 2015
Accepted 13 August 2015
Available online 28 August 2015

Keywords:
Energy balance closure
Soil heat flux
Eddy covariance

ABSTRACT

Quantifying uncertainty in determining the surface soil heat fluxes (G_0) to close the surface energy balance in micrometeorological studies remains an open question. While numerous methods have been proposed to determine G_0 and have been validated individually, few studies have cross-evaluated these methods to examine how the derived G_0 from different methods affects the closure of the surface energy balance. Using data measured at an arid shrub-land site during summertime, nine different methods were evaluated ranging from conventional heat-storage calorimetry to methods derived directly from the heat transfer equation. Apart from the entire dataset, two subsets were used; one with minimal variation from idealized diurnal radiation cycles and the other with highly variable radiation conditions. Under the entire dataset, the performance of the methods varied while there was a distinct drop-off in the level of closure under the variable radiation conditions. The methods that allowed for the most variation in inputs between time steps performed better than those that used diurnal or constant input values. Because of this, a calorimetry method and Green's function-based method are more highly recommended than other methods.

1. Introduction

The surface energy imbalance in micrometeorological studies remains an unsolved problem (Foken et al., 2011). At most flux sites, the sum of the sensible heat (H) and latent heat (LE) fluxes is on average 10–30% less than the available energy ($A = R_n - G_0 - S$ where R_n is the surface net radiation, G_0 is the soil heat flux at the surface, and S is changes in heat storage in the air and vegetation below the flux measurement height) (Wilson et al., 2002; Liebethal et al., 2005; Foken, 2008; Cava et al., 2008; Jacobs et al., 2008; Gentine et al., 2012; Stoy et al., 2013). Theoretical, instrumental, and methodological reasons have been proposed to explain the reasoning for the observed energy imbalance problem in the surface energy budget. This includes instrument footprint-scale mismatch, advective flux divergence, low frequency and large scale turbulent motions, and measurement and calculation errors in all components of the surface energy balance (e.g., Wilson et al., 2002; Mauder et al., 2007; Oncley et al., 2007; Foken, 2008; Foken et al., 2011; Leuning et al., 2012; Wohlfahrt and Widmoser, 2013).

Efforts have been made to examine the influence of the potential error sources on the lack of energy closure. Even with careful consideration and investigation of experimental design, post-field data processing and instrumentation, lack of energy closure is still reported (Mauder and Foken, 2006; Kohsiek et al., 2007; Mauder et al., 2007; Oncley et al., 2007; Cava et al., 2008; Foken, 2008; Leuning et al., 2012; Wohlfahrt and Widmoser, 2013) even though measurements, flux corrections and, data processing have been studied extensively (Mauder and Foken, 2006; Oncley et al., 2007; Kohsiek et al., 2007; Mauder et al., 2007). Of the terms in the energy balance, R_n is a relatively accurate term with at most a 5% error (Kohsiek et al., 2007). Mauder and Foken (2006) found that rigorous post-field data processing and flux calculation can reduce the energy balance residuals up to 17%. If appropriate corrections are used, then the errors within the sensible and latent flux calculations can be minimized so their impact upon the overall energy balance imbalance is reduced leaving G_0 as a potential source of systematic error.

Soil heat flux is commonly measured by soil heat flux plates at some depth (Z_m) below the surface (G_{zm}). Because of this, changes in the heat storage in the soil layer above the heat flux plates (S_G) needs to be determined G_0 ($G_0 = G_{zm} + S_G$). Some methods of calculating G_0 do not require an S_G term because they calculate G_0 directly at the surface using the thermal properties of the soil

* Corresponding author. Tel.: +1 509 335 1529; fax: +1 509 335 7632.
E-mail address: Heping.Liu@wsu.edu (H. Liu).

http://dx.doi.org/10.1016/j.agrformet.2015.08.255
0168-1923/

seeded by direct measurements. G_{zm} has to be measured deep enough in the soil so the flux plate and other instruments are not affected (Mayocchi and Bristow, 1995; Wang and Bras, 1999; Kustas et al., 2000; Ochsner et al., 2007; Gentine et al., 2012; Sun et al., 2013). However, G_{zm} becomes damped and lagged by the soil layer between Z_m and the surface (Z_o) compared to G_0 (Oncley et al., 2007; Foken, 2008; Gao et al., 2010; Sun et al., 2013; Li et al., 2014). Placing heat flux plates very near the surface (within a few millimeters of the surface) is not advisable as the overlying soil can lose contact with the rest of the near-surface soil matrix adversely affecting water and heat flow (Mayocchi and Bristow, 1995; Wang and Bras, 1999; Ochsner et al., 2007; Núnez et al., 2010; Leuning et al., 2012). Burying the soil heat flux plate forces an accounting for S_G since it can be as large as the measured in-soil heat flux (Mayocchi and Bristow, 1995; Kustas et al., 2000; Heuskinveld et al., 2004; Yang and Wang, 2008; Foken, 2008; Hsieh et al., 2009; Higgins, 2012) but quantifying S_G is site specific due to differences in vegetation, soil, and topography across different landscape (Cava et al., 2008).

Multiple methods exist to calculate G_0 from G_{zm} to soil and surface temperatures. Calorimetry is the typical field-based method but it requires significant knowledge about the site's soil characteristics and multiple in-soil measurements. Other methods require only one measurement (surface temperature or G_{zm}) and minimal knowledge of soil properties. The use of the best methods to calculate G_0 can reduce uncertainty in the overall energy balance and identify the causes for the lack of closure at micrometeorological flux sites. Previous studies have examined individual aspects of how different calculation methods affect the soil heat flux estimates such as phase lag (Gao et al., 2010; Sun et al., 2013), missing energy pathways (Higgins, 2012), and variation in the incoming radiation (Gentine et al., 2012). Similar analyses have also been done as parts of large field campaigns (e.g. EBEX) (Oncley et al., 2007) and general reviews regarding the energy budget closure problem (e.g., Foken, 2008; Leuning et al., 2012).

As newer methods to calculate G_0 are derived and proposed, they are compared to calorimetry as validation then used in energy balance calculations to test their efficacy. However, few studies have compared multiple methods and the ones used in these studies have minimal overlap (e.g., Liebethal and Foken, 2007; Venegas et al., 2013; Li et al., 2014). Nine different methods to calculate the soil surface heat flux are presented and compared; each requiring different input soil parameters and measurements. There are similarities between some of the methods but all are treated independently. The objective is to compare the practical applications of each method and their ability to close the energy balance for a typical experimental set-up and flux calculations. The focus of this study is not on identifying and reducing possible error sources from other components of the surface energy balance equation (i.e., H, LE, and R_n) or on deriving and improving the methods presented. Therefore, discussion of the turbulence or stability conditions or of measurement and flux correction errors is beyond the scope of this study. Section 2 describes the data and site used, Section 3 gives an overview of the methods and analysis used, Section 4 presents the results, Section 5 discusses the issues that affected the closure rates and G_0 calculations and recommends the best methods, and conclusions are in Section 6.

2. Data

2.1. Experiment site

Data were collected from an eddy-covariance tower located in the Birch Creek Valley in southeast Idaho (44°08'48"N, 112°57'10"W) from June 25, 2013 until September 15, 2013. The site had short, intermittent vegetation cover comprised mainly of sagebrush no taller than 0.75 m with scattered short grasses between and around the brush. Fig. 1 is an image of the valley and a picture of the tower at the site. The terrain overall sloped approximately 5% from the north to the south with mountains located to the west (4.5 km to peaks) and east (5.5 km to peaks) of the tower. The terrain locally sloped downward to the east toward the center axis of the valley. The soil around the tower site was a sandy-loam with a population of stones and gravel within the matrix. The eddy covariance systems on the tower consisted of a sonic anemometer (model CSAT3, Campbell Scientific Inc.) and open-path infrared gas analyzer (model LI7500A, LiCor Inc.) at 3 m, with a co-located temperature/relative humidity sensor (HMP45C, Campbell Scientific, Inc.). Also used were a net radiometer (7.5 m, CNR2, Kipp & Zonen) and downward looking infrared thermometer (3.5 m, SI-111 Apogee Instruments Inc.). Buried near the tower was an array of soil sensors including seven soil temperature sensors (0.025, 0.05, 0.075, 0.10, 0.15, 0.20, and 0.25 m, 109SS, Campbell Scientific Inc.), five volumetric water content reflectometers (0.025, 0.05, 0.10, 0.15, and 0.20 m, CS616, Campbell Scientific Inc.), and two self-calibrating soil heat flux plates at 0.06 m (HFPSC-01, HuskeFlux Thermal Sensors).

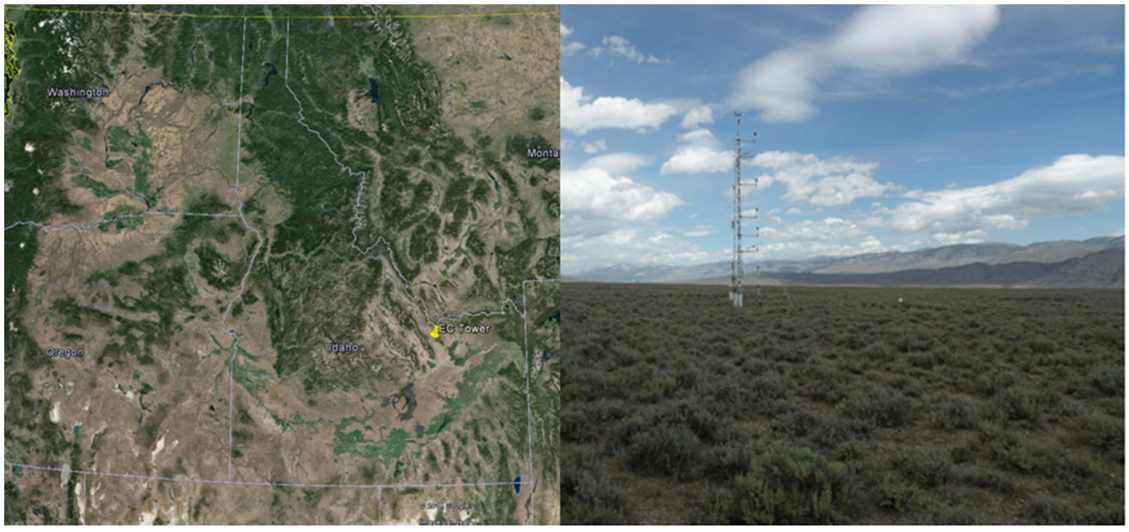

Fig. 1. Google Earth image of the overall valley with the site denoted by the pin (left) and picture of the measurement site looking to the north (right).

Table 1
Method, input measurements, soil properties, formula base, and reference papers for each method. Like methods are shaded together.

Method	Measurements (Number)	Input soil properties	Formula base	References
Calorimetry (CAL)	G_z, T_s, T_z, VWC (4 minimum)	Bulk density, soil mineral specific heat, soil mineral density	1-D Calorimetry from heat conduction equation	Liebethal et al. (2005), Oncley et al. (2007), Foken (2008), Leuning et al. (2012), Venegas et al. (2013) and Li et al. (2014)
SM	G_z, T_s, T_z, VWC (4)	Bulk density, soil mineral specific heat, soil mineral density	Same as CAL	Liebethal and Foken (2007)
G10	T_s (1)	Thermal diffusivity and conductivity	Diurnal sinusoidal wave from thermal conduction and convection	Gao et al. (2010) and Li et al. (2014)
WBZ12-S	G_z (1)	Thermal diffusivity	Diurnal sinusoidal wave	Wang and Bou-Zeid (2012)
H04	T_s (1)	Thermal diffusivity and conductivity	Harmonic-based diurnal sinusoidal wave, same base as G10	Heusinkveld et al. (2004) and Li et al. (2014)
UFG	T_s, R_n (2)	None	Empirical percentage between R_n, n, and G_0	Santanello and Friedl (2003) and Liebethal and Foken (2007)
L12	G_z, T_s, T_z (3)	None	Harmonic-based damping depth	Leuning et al. (2012)
H09	T_s, VWC (2)	Bulk density, specific heat, soil density, thermal conductivity	Half-order time derivative from 1-D heat diffusion equation	Wang and Bras (1999) and Hsieh et al. (2009)
WBZ12-G	G_z or T_s (1)	Thermal diffusivity	Green's function derivation of 1-D heat conduction equation	Wang and Bou-Zeid (2012)

2.2. Data correction and selection

The eddy covariance data were collected at 10 Hz while the meteorological data were stored as 30 min averages from 1 s samples (not available). Half-hour latent and sensible heat fluxes were calculated from the eddy covariance data. The coordinate system was rotated via the planar fit method (Wilczak et al., 2001), sonic temperature corrected for water vapor (Schotanus et al., 1983), and latent heat flux for density effects (Webb et al., 1980). Prior to these corrections the data were despiked (Vickers and Mahrt, 1997) and checked for physical realness based on sensor limits. Three days were removed from the data set (July 5–7) due to missing and bad data. Three sets of data were used to test the efficacy of the surface soil heat flux calculation methodologies with respect to closure. The first was the entire data set to examine how well the methods worked under multiple conditions as a whole (hereafter ALL). The second was ten non-consecutive days where the net radiation data showed a smooth curve indicating no cloud passage (hereafter SUN). The final was a set of 9 non-consecutive days that showed a high degree of variability within the net radiation (hereafter CLOUD). The goal with these three sets was to span the range of possible radiation conditions (variable to "idealized") and isolate each group to investigate how the different methodologies handle the possible range of variation within the radiation conditions. Also, this will show how the different methodologies respond to non-ideal conditions, both for consecutive (ALL) and non-consecutive periods (CLOUD, SUN).

2.3. Methodologies and technical treatments

Nine different methodologies were used to calculate G_0 and the associated energy balance closure rates along with not using any correction/calculation (hereafter NONE) for the soil heat storage. The method names, input parameters, needed measurements, formula basis, and references are listed in Table 1. The equations and a short description for each method are provided in Appendix A. These methods were selected due to their being field-based and having relatively simple parameterizations with expectation of good performance based upon their evaluations to date. Due to the general underestimation of the flux values overnight from the sine-wave assumptions, the overnight values for the sinusoid-based methods (G10, H04, and WBZ12-S) were set to G_{zm} starting at sunset (~18:00 local time) and ending at sunrise (~05:30 local time) (Gao et al., 2010). Soil thermal diffusivity and thermal conductivity are assumed to be constant through the soil layer. The level of closure was determined through the slope of an orthogonal linear regression between available energy ($R_n - G$) and the turbulent fluxes ($H + LE$) with the intercept of the regression line acting as an offset. The coefficient of determination (R^2) for each fit line is provided as a measure of the amount of scatter and uncertainty for closure for a particular method.

Table 2
Input soil characteristics and thermal properties.

Variable	Value
Bulk density	1.53 g m^3
Specific heat of minerals	870 J g^{-1} K^{-1}
Density of minerals	2.65 g m^3
Soil thermal conductivity	0.854 W m^{-1} K^{-1}
Soil thermal diffusivity	2.947×10^{-7} m^2 s^{-1}

The input soil properties are listed in Table 2 and were kept constant for all methods and calculated prior to the G_0 calculations. The soil thermal diffusivity (k) was calculated by equating the damping depth from L12 (Eq. A5), with the general form of damping depth ($\sqrt{2k/\omega}$) and solving for k. This value was then used in G10 which was solved for soil thermal conductivity (λ) at the same depth as the soil flux plates using the known G_{zm} values. Thermal diffusivity and conductivity can vary in time with water content and temperature but given the minimal variation in the soil water content (not shown) and normal temperature conditions, these variations can be ignored (Hillel, 2004). Liebethal et al. (2005) showed that for a ±50% variation in λ, the effect on G_0 is relatively small so mean values of k and λ were used over the entire data set.

Eq. A2 was used to calculate the soil volumetric heat capacity; the effect of air and organic materials within the soil were neglected. The bulk density of the soil came from the USDA Web Soil Survey (websoilsurvey.sc.egov.usda.gov, tabular and spatial data from Dec 10, 2013) using the GPS coordinates of the tower. The density and specific heat of soil minerals were obtained from Campbell and Norman (Campbell and Norman, 1998, Table 8.2, pp. 118). The other input parameters for each method were either directly measured (soil heat flux, depth, soil surface temperature [T_S], soil

water content), inherent constants in the method, or calculated via the requirements of the method. CAL is used here as a reference method due to its prevalence as the preferred method in the literature. The reader is referred to the referenced papers for more explicit details regarding the derivation and source of each methodology.

Phasing for each method was considered specific to each method. The phase for five of the methods (H09, WBZ12-G, UFG, SM, and CAL) were inherent to their calculation. Two methods (L12, H04) included a specific phase adjustment. The final two methods (G10, WBZ12-S) gave a base phase value within the sine function but was adjusted to minimize the hysteresis curve using advice from Ochsner et al. (2007) (Eq. (A6)) and Sun et al. (2013) (Eq. (18)).

3. Results

3.1. Radiation and flux conditions

Fig. 2 shows the mean diurnal net radiation, and sensible and latent heat fluxes for the three data sets (ALL, SUN, and CLOUD). Under the ALL conditions, values average to smooth curves though there is a high degree of variation in the individual days. A similar mean picture is seen under the SUN conditions as these days were chosen because of the minimal visible, short-term variability in the particular day's R_n. This provides a set of more "idealized" days in hope to achieve the best possible closure rates for each method and minimize impacts from variation in the 30 min data in the incoming radiation. The mean CLOUD conditions show a purposefully more variable pattern than SUN or ALL to determine if the methods can handle higher degrees of variability in R_n. The mean ALL radiation

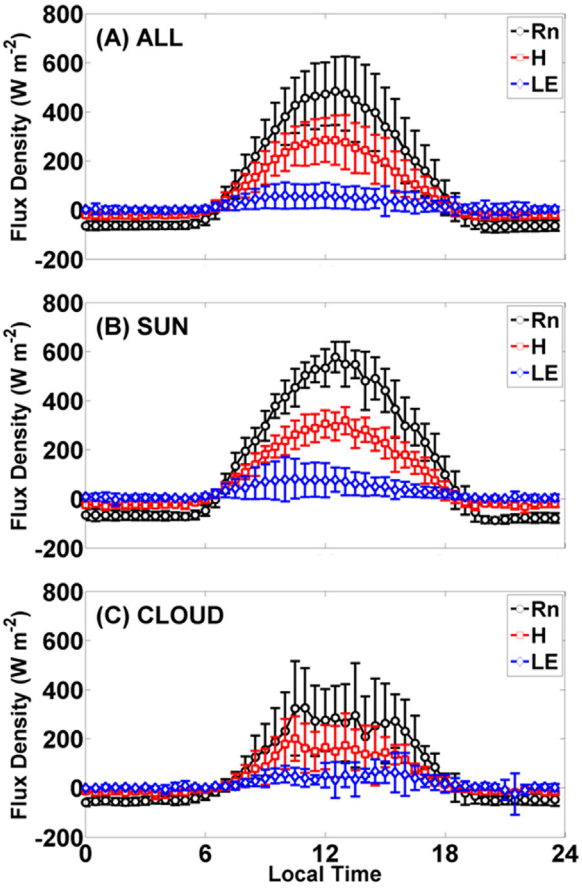

Fig. 2. Mean energy fluxes and net radiation for ALL (A), SUN (B) and CLOUD (C). Error bars represent one standard deviation from the mean value.

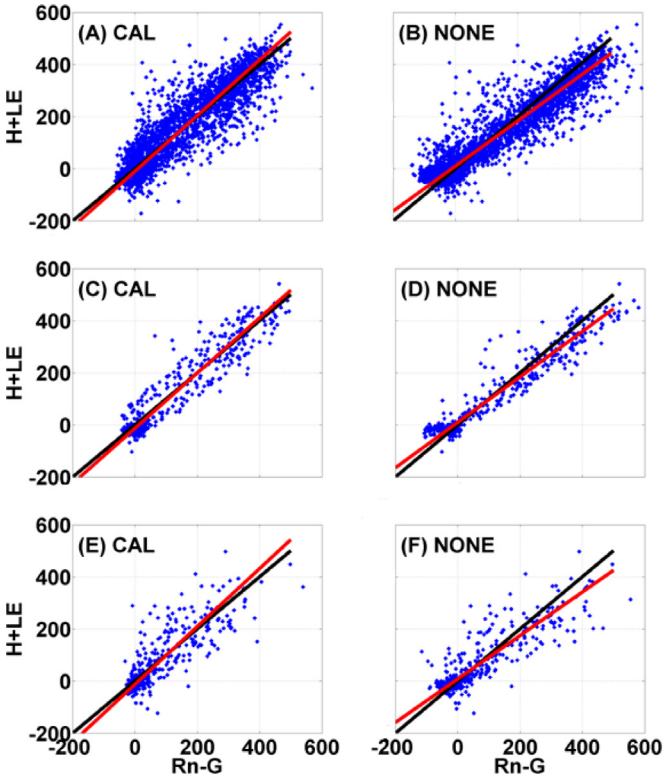

Fig. 3. Scatter plots comparing the available energy ($R_n - G$) to the turbulent energy fluxes ($H + LE$) for CAL (A, C, E) and NONE under ALL (A,B), SUN (C,D), and CLOUD (E,F). The slope and goodness of fit for each line is noted in the figure with the intercept forced to zero. The red line is the linear best fit with the reported slope while the black line is a 1:1 line(For interpretation of the references to color in this figure legend, the reader is referred to the web version of this article).

conditions are similar to those in SUN though the individual days maintain the full range of variability not present in SUN. From this, the expectation is that ALL and SUN will have similar closure rates due to the similarities of the mean values with CLOUD differing because of the different shape of its mean R_n.

3.2. Comparison between calorimetry and NONE

Fig. 3 shows the comparison of the 30 min means for CAL with NONE via scatter plots under the different subsets with the linear regression. CAL performs well across the different conditions with high levels of closure as for both SUN and ALL closure was within 7%. Under CLOUD, the level of closure moved further from unity to 1.11 and 0.83 for CAL and NONE, respectively, with scatter increasing for both. Though the overall closure with CAL is higher than NONE in each subset (Table 3) there is more scatter for CAL than in NONE. The overall performance is better under SUN than under CLOUD where the more variable radiation can cause issues with the phase shift due to the lag time between the surface and measurement depth (Sun et al., 2013). The average radiation curve for ALL was more similar to SUN than CLOUD. For shorter data sets, the incoming radiation conditions play an important role on the level of energy balance closure. When using shorter data sets with more variable radiation, not capturing the variability can cause lower levels of closure. This same behavior is reflected in both CAL and NONE with the radiation conditions adversely affecting the closure rates. Under the SUN conditions, some imbalance still remains though less than under CLOUD or ALL. The source of this imbalance could be from other aspects of the energy budget analysis and is beyond the scope of our discussion.

Table 3
Linear fit statistics for ALL, SUN, and CLOUD for half-hour time periods and daily closure rate.

	ALL			SUN			CLOUD			DAILY		
Method	Slope	Intercept	R^2	Slope	Intercept	R^2	Slope	Intercept	R^2	Slope	Intercept	R^2
CAL	1.07	−9.93	0.84	1.06	−13.02	0.89	1.11	−12.49	0.69	1.04	−7.13	0.89
G10	1.10	31.84	0.80	1.07	28.10	0.87	1.08	33.16	0.56	0.91	43.30	0.78
L12	1.36	−18.58	0.72	1.41	−31.07	0.80	1.47	−27.98	0.42	1.06	6.27	0.57
H04	1.25	34.85	0.68	1.24	25.86	0.75	1.11	45.75	0.39	0.89	52.75	0.79
H09	1.19	−34.89	0.74	1.11	−33.08	0.77	1.29	−35.15	0.62	0.96	−9.17	0.90
WBZ12-S	1.00	25.27	0.84	1.03	22.03	0.90	1.01	23.83	0.63	1.00	25.27	0.92
WBZ12-G	0.95	−3.56	0.88	0.95	−6.71	0.92	0.91	−0.55	0.73	0.95	−3.56	0.93
UFG	0.92	23.53	0.91	0.89	29.40	0.94	0.88	18.61	0.80	2.24	12.32	0.60
SM	1.15	−17.36	0.84	1.13	−21.47	0.88	1.24	−20.72	0.72	1.03	−6.14	0.89
NONE	0.86	9.93	0.88	0.87	9.56	0.92	0.83	7.71	0.74	1.00	−3.38	0.90

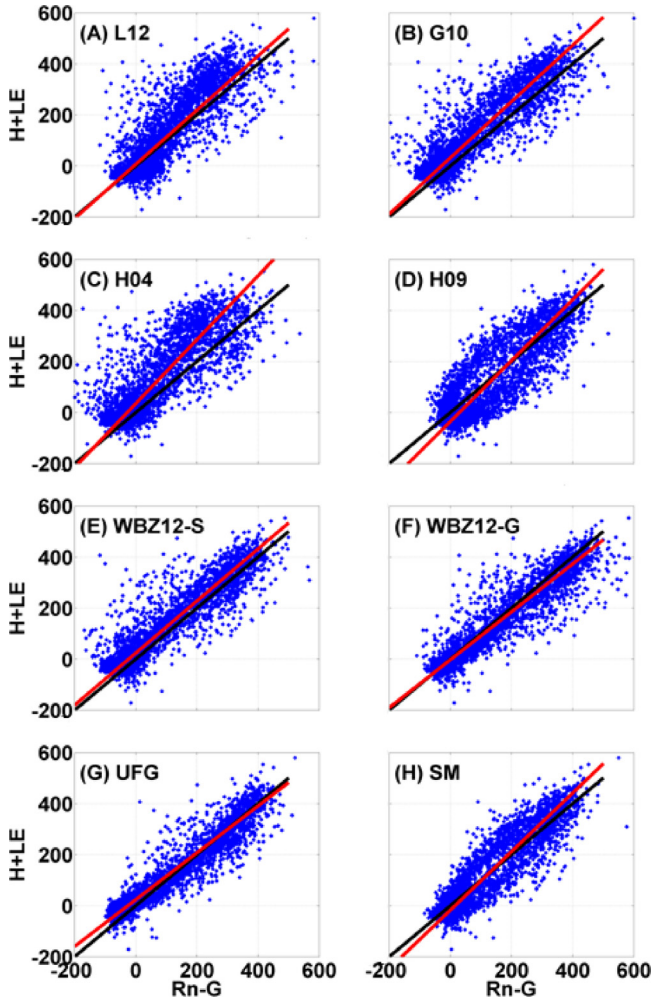

Fig. 4. Scatter plots comparing the available energy ($R_n - G$) to the turbulent energy fluxes ($H + LE$) for each method (L12 [A], G10 [B], H04 [C], H09 [D], WBZ12-S [E], WBZ12-G [F], UFG [G], and SM [H]) under ALL. The slope and goodness of fit for each line is noted in the figure with the intercept forced to zero. The red line is the linear best fit with the reported slope while the black line is a 1:1 line.

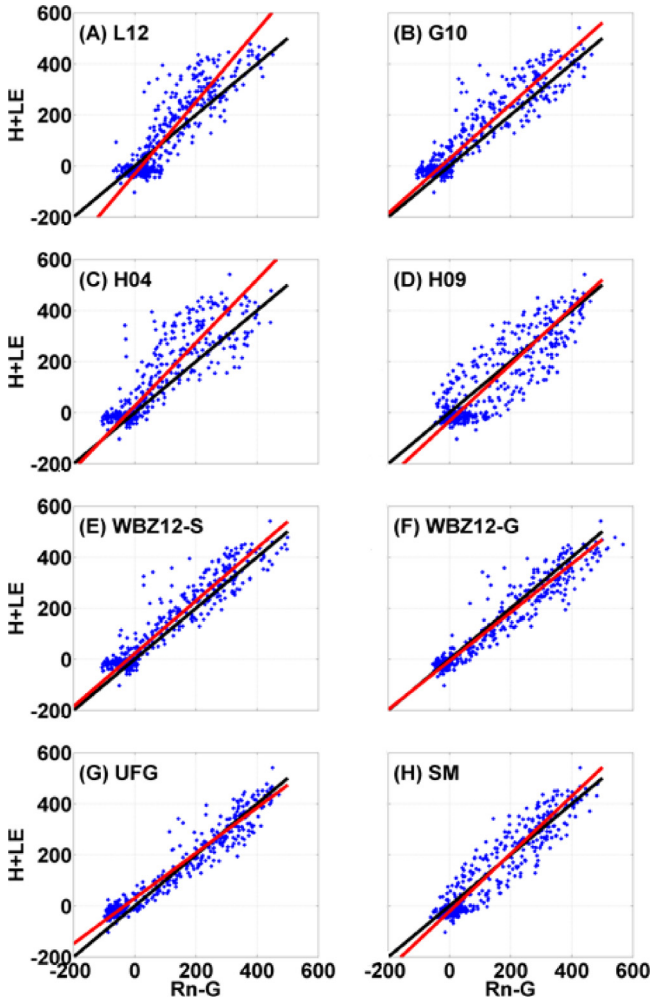

Fig. 5. Scatter plots comparing the available energy ($R_n - G$) to the turbulent energy fluxes ($H + LE$) for each method (L12 [A], G10 [B], H04 [C], H09 [D], WBZ12-S [E], WBZ12-G [F], UFG [G], and SM [H]) under SUN. The slope and goodness of fit for each line is noted in the figure with the intercept forced to zero. The red line is the linear best fit with the reported slope while the black line is a 1:1 line.

3.3. Comparison of alternative methods

Figs. 4–6 show the scatter plots of the 30 min means for the other methods under the data sets. A summary of the fit statistics are presented in Table 3. Similar to CAL, scatter increased for all methods under CLOUD conditions with the increased variability in net radiation. SUN showed the highest levels of closure though there was variability in the closure levels across the methods. Six methods (L12, H04, WBZ12-S, H09, G10, and SM) in ALL had closure levels >1. L12 and H04 showed the largest variability across the different data sets with the worst estimates of closure for SUN and ALL. H09 and SM did worse than H04 for CLOUD. The use of harmonics in H04 was expected to maintain a higher level of closure during the periods of higher net radiation variability but was not successful in this study (Fig. 7). WBZ12-S and G10 were relatively consistent with their slope and intercept across conditions. The mean net radiation for CLOUD was not replicated by the sinusoid methods (Fig. 7) but was not detrimental to the end closure rates.

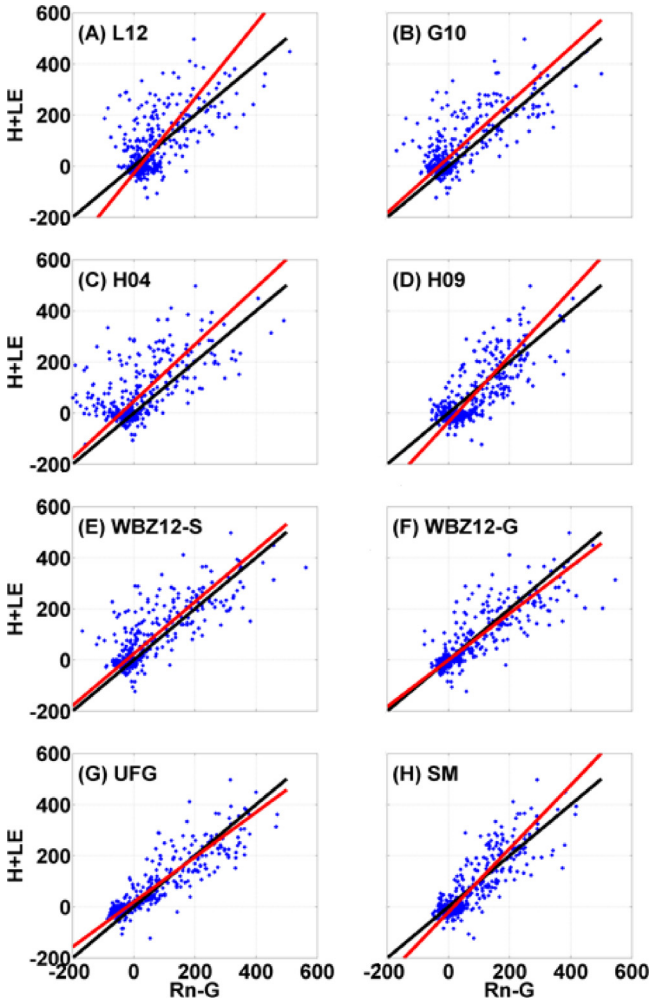

Fig. 6. Scatter plots comparing the available energy ($R_n - G$) to the turbulent energy fluxes ($H + LE$) for each method (L12 [A], G10 [B], H04 [C], H09 [D], WBZ12-S [E], WBZ12-G [F], UFG [G], and SM [H]) under CLOUD. The slope and goodness of fit for each line is noted in the figure with the intercept forced to zero. The red line is the linear best fit with the reported slope while the black line is a 1:1 line.

WBZ12-G and H09, though mathematically equivalent (Wang, 2012), did not perform the same due to the difference in the input variables and their inherent qualities. WBZ12-G had less scatter than H09 and its closure levels were more consistent than H09 which had an issue with the downslope side of the diurnal wave having the lowest G_0 values during the early evening and overnight (Fig. 7). There was an issue with H09's phasing as well, being ahead compared to other methods (Section 5.2). UFG and WBZ12-G had delayed maximum G_0 as the heating in the morning of their curves was delayed compared to the other methods. Even so, UFG had consistent closure rates across the subsets. SM did not perform as well as its cousin method (CAL) in part from the increased range of values per splitting the temperatures into two layers (see A.9) but did not disrupt its scatter. CAL performed relatively well when taking the combination of slope/intercept into account. Its slope was not the nearest to unity but had some of the lowest intercept values. Closure could be improved by using more specific site-measured values for all the soil characteristic inputs.

3.4. Daily closure values

Daily closure was calculated by averaging LE, H, R_n, and G_0 over the course of a day then comparing the averaged values so each day was condensed to a single comparison point. Fig. 8 shows the daily closure for each method for the three conditions. A different picture arises in the daily closure rates than the individual half-hour points. The three sine methods resulted in an underestimation of total energy balance assuming that the turbulent fluxes at daily averages are not significantly underestimated. If H and LE are underestimated at a daily scale then the behavior in the sine methods might be significant miss-representation of G_0 given potential error in other terms. This would also shift the majority of methods (CAL, SM, H09, L12, and WBZ12-G) to underestimating G_0 since as they sit closer to unity. The further away from unity a method's slope was, the larger the improvement between the half-hour and daily averaging. Most intercepts were pulled closer to zero but not as consistently or as significantly as the slopes (Table 3). UFG was unique since the overestimation increased with increasing turbulent heat fluxes. This causes concern in its usefulness at a daily timescale even though this issue did not present itself at half-hour

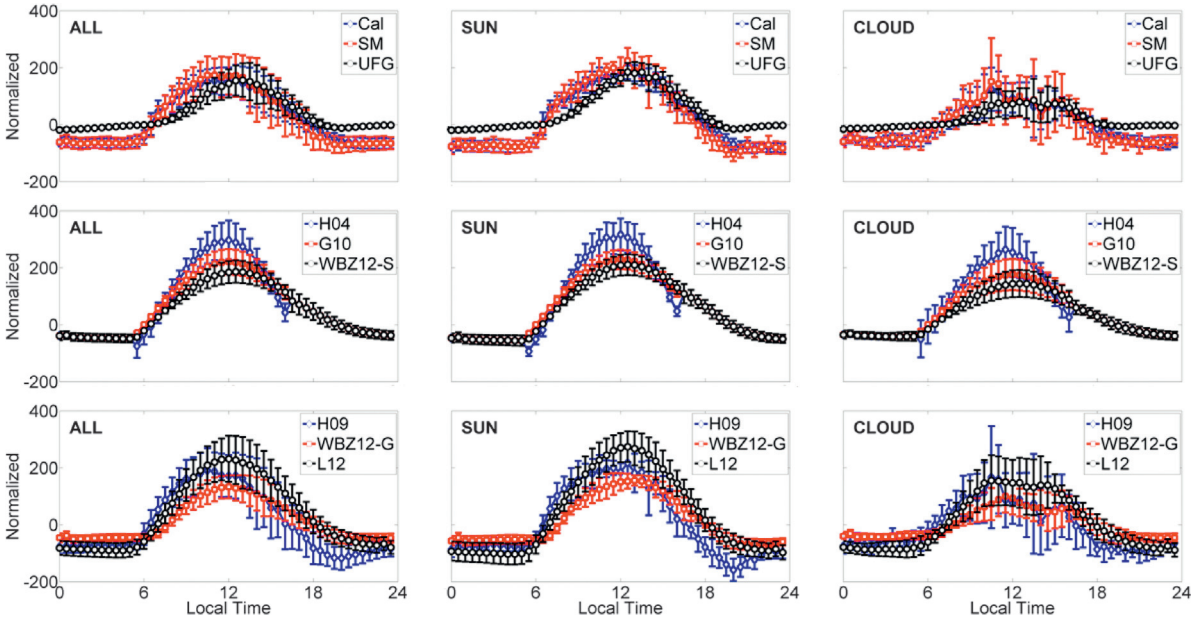

Fig. 7. Calculated soil surface heat flux for all methods under the three data sets (ALL [A], SUN [B], and CLOUD [C]).

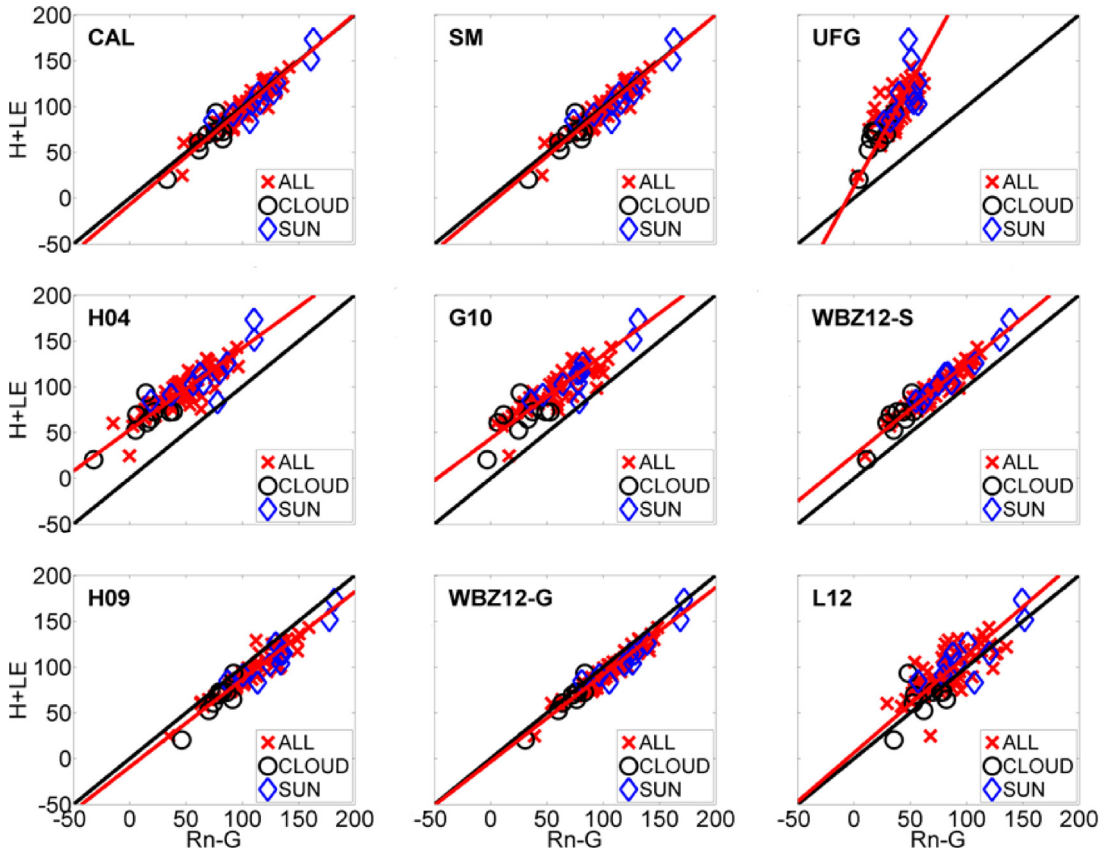

Fig. 8. Daily closure for each method for the three data sets: ALL (red x), CLOUD (green circle), and SUN (blue triangles). ALL includes the points from CLOUD and SUN. The red line represents the orthogonal linear best fit and the black line is the 1:1 line.

scales (Figs. 4–6). For all but UFG, the closure rates improved over the half-hour scale so the lengthening of the timescale did improve upon the end closure. UFG's issue comes from the overnight values of G_0 not being negative enough in relation to the rest of the methods (Fig. 7) therefore not reflecting a more realistic surface heat loss during the night. For this reason, UFG would not be a strong choice as an all-inclusive method without a specific adjustment for the overnight periods. Daytime, it is adequate in current form but not for overnight.

At daily averages, the difference is limited to the magnitude of the average of the overall energy though the high end of CLOUD and low end of SUN do marginally overlap. CLOUD days do not show a worse fit compared to SUN or ALL lending support to the fact that if closure is going to be attempted at shorter timescales then the variability in the net radiation between time steps needs to be accounted for. Over the course of a day, variability can be averaged out which is why the CLOUD days do not show the same scatter as at the half-hour timescales. Daily averaging removes the issue of phasing since any mismatch gets buried within the averaging.

4. Discussion

4.1. Diurnal evolution of G_0

The methods that allowed for the most variation between time steps with minimal diurnal-based values (CAL, SM, WBZ12-G, and H09) tended to perform better than those that used diurnal-based values (G10, H04, L12, UFG, and WBZ12-S) based off the 30 min averages. Use of diurnal or averaged terms limited the range of values that could be produced by a method disallowing G_0 values to adapt to changing conditions. Under SUN, the variability between consecutive half-hour time-steps was low so allowable variation did not have as strong of an impact upon the final closure rates as under CLOUD. The sinusoid methods showed smoother curves (Fig. 7, middle row) even though H, LE, and R_n were not smooth under CLOUD (Fig. 2). On non-idealized days, G_0 will be overestimated, underestimating the available energy for the turbulent fluxes. WBZ12-S had the lowest values of this group because it used G_z instead of T_s for its amplitude. The drawback of the sinusoid methods is seen in CLOUD as they produced smooth mean curves unlike the mean R_n. This difference helps explain the relatively large slopes, particularly in the daily closure for G10, H04, and WBZ12-S (Fig. 8). If an overnight adjustment was not made, then the continuation of the sine-curve would cause worse problems by overestimating the heat loss from the soil.

UFG and L12 used diurnal-based variables but combined with time-step based values so they were able to capture some of the R_n variability. UFG did not capture the overnight values, with its magnitude being larger than the other methods. It also had trouble with the "warm-up" part of the day, presenting a shallower slope though eventually reaching maximum values akin to CAL and SM and following their path until about 18:00 LT; its phasing will be discussed in more detail in Section 5.2. Suffice to say here, this caused its lower closure levels at daily scales but its daytime performance offset this so its overall half-hour closure was not significantly impaired. WBZ12-G also had a delayed maximum but the impact was less than UFG's. The expectation was WBZ12-G would be similar to H09 but this was not the case, likely because the input variables used (G_z vs. T_s) have different levels of variability upon the amount of damping done by the soil. The other difference is in regard to the time-step influence in these two methods but this will be discussed in Section 5.2.

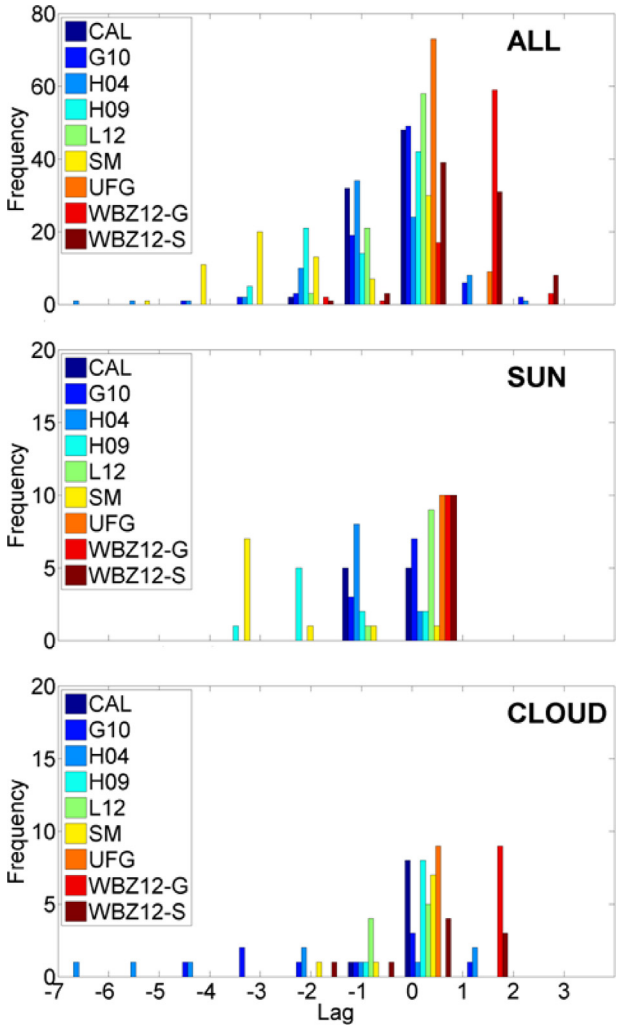

Fig. 9. Frequency of lag time from the cross-correlation between R_n and G_0.

CAL and SM had very similar time-evolutions due to their similar calculations. The range of values was larger for SM during the daytime but the two were similar overnight. The daytime differences were enough to move SM further from overall closure than CAL for the half-hour time periods but at daily scales, the difference was minimal. What is most evident from these two methods is a more rapid increase of G_0 in the morning compared to a more general decrease in the afternoon. This was seen in H09, L12, and WBZ12-G as well but not as sharply. CAL and SM more adequately captured the changes in the mean R_n for CLOUD (Fig. 7) than most of the other methods with a smoother portion of the daytime G_0 differing from the shape of R_n (Fig. 2).

4.2. Phasing and variability

To assess the phase lag, the cross correlation between the different G_0 calculations and R_n were calculated. The data were normalized by the maximum value for the particular day, and the biased cross-correlation was then taken for each day with a 10 step lag (5 h). All the methods maximize the cross-correlation typically within an hour of the zero lag but not all reach their maximum at the zero lag (Fig. 9; Table 4). Only H04 (−1 lag) and WBZ12-G (+1 lag) did not have the mean maximum correlation at the zero lag. The calculated G_0 flux is primarily in phase with the R_n so phasing was not a significant issue for most of the methods. There is some variability around the center point and the degree of variability is due to a small number of points (Fig. 9). Three methods (UFG, WBZ12-G, and WBZ12-S) had a positive mean lag, which means that G_0 led R_n and for the rest, R_n was ahead of G_0. There were only four times the lag exceeded 1.5 h, three for H04 and once for G10; otherwise all the other methods were within ±3 lags. Four methods (SM, L12, CAL, and H09) never had a positive lag so their phase was either the same or lagged behind the incoming radiation. UFG did not have a negative lag so it was never behind R_n. The rest (G10, H04, WBZ12-S, and WBZ12-G) straddled zero lag. G10 and H04 had a wider range but this was from singular times. Fig. 9 shows that the mean values in Table 4 are deceptive because the variability in the lag comes from only a few points for any given method.

L12 was the only method where the phase shift is independent of the G_0 calculation, implemented by shifting the entire trace in time by the ratio of the measurement depth to the damping depth calculated from the soil temperature wave (see Section A.4). The sinusoid based functions (G10, H04, and WBZ12-S) have more rigid phase considerations due to the sine wave phase variable. The other methods had no specific phase variable. Sun et al. (2013) explored the issue of phasing (hysteresis) between R_n and G_0 providing a physical range ($\pm\pi/4$) on the phase shift between R_n, surface temperature and G_0. The limit works as a first approximation at arid sites because of the minimal influence of soil moisture upon the thermodynamics of the soil matrix, but the presence of any water in soil would affect the phase shift by affecting the heat transfer through the heat capacity of the soil matrix.

The phase limit implies that there should be not more than a 3 h difference between the net radiation measurement and the surface soil heat flux response. This is equivalent to a ±6 lag in the cross-correlation analysis done here. For SUN, all but H09 were consistently within ±1 of zero whereas for CLOUD, there is a larger spread but is limited to the sinusoid methods per their more rigid phasing. G10 and WBZ12-S both maintain a constant phase shift while H04 is somewhat variable (A.3). Using a more dynamic phase variable for the sinusoid methods could remove the more extreme lags seen but it would not address matching the variability at sub-daily timescales. For the other methods, so long as timing is consistent and correct when calculating G_0 then phasing should not be an issue.

H09 and WBZ12-G had some of the highest mean and variation in their lag times, but both have calculations dependent on neighboring time-steps. Their lags are opposite signs because H09 uses information from $t+1$ while WBZ12-G uses calculations from $t-1$ so they behave oppositely through the influence of the antecedent or subsequent values (see Eqs. A8, A9, and A11). UFG's phasing is accomplished through a cosine wave that is adjusted by the timing of solar noon and amplitude from a function of the amplitude to the surface temperature and R_n. CAL and SM have no inherent phase or timing considerations, responding directly to the way the soil temperature and moisture change over time.

The impact of phasing on the final closure rates depended upon the time-scale of interest. The higher degree of scatter within the sinusoid methods seen during CLOUD could, in part, be due to some phasing mismatch but could have resulted from the influence of clouds on the timing of the maximum R_n. This returns the problem of being able to capture the variability at sub-daily time-steps. For all others, the phasing for CLOUD and SUN were similar and relatively consistent with ALL. Phasing impacts closure rates at sub-daily timescales but averaging at daily scales removes its impact. For example, UFG had the best overall phasing match but the worst daily closure levels whereas WBZ12-G had a worse phasing match but higher daily closure. If using a smaller subset with specific characteristics (e.g., CLOUD or SUN), then phasing can have an impact depending upon the method but is most detrimental to the sinusoid methods.

Table 4
Mean and standard deviation for the cross-correlation between R_n and G_0 for the nine different methods representing hour lag times.

	ALL	SUN	CLOUD
Method	Mean ± Standard deviation	Mean ± Standard deviation	Mean ± Standard deviation
CAL	−0.44 ± 0.55	−0.5 ± 0.53	−0.11 ± 0.33
G10	v0.30 ± 0.94	−0.3 ± 0.48	−1.33 ± 1.73
H04	−0.80 ± 1.32	−0.8 ± 0.42	−2.11 ± 2.76
H09	−0.87 ± 1.00	−1.5 ± 0.97	−0.11 ± 0.33
L12	−0.33 ± 0.55	−0.1 ± 0.32	−0.44 ± 0.53
SM	−0.40 ± 0.65	−0.6 ± 0.52	0 ± 0
UFG	0.11 ± 0.31	0.2 ± 0.42	0 ± 0
WBZ12-G	0.73 ± 0.67	0.5 ± 0.53	1.22 ± 0.44
WBZ12-S	0.54 ± 0.83	0.2 ± 0.42	0.11 ± 1.17

4.3. Performance and recommendation

CAL and SM have very similar formulations in that they both account for the heat storage in the soil layer above the heat flux plate. Li et al. (2014) saw CAL overestimate the amplitude of the heat storage but, like here, it (and SM) was able to handle variability across each time step. Liebethal and Foken (2007) deemed the SM method as one of the two best of six in their study. The only drawback is they require the most soil information. Of sinusoid methods, H04 performed the worst with WBZ12-S and G10 having better performances. H04 was deemed better than the CAL equivalent in Li et al. (2014) because it captured the diurnal variation in the soil heat wave in their study, but performed the worst here. Li et al. (2014) also used half-hour time-steps but noted that the data was collected under "fine weather conditions". Heusinkveld et al. (2004) used 15 min values and noted that the measuring interval needs to be no more than 15 min given the possible dynamic variability in the soil heat flux. This leaves open the question of how frequent soil measurements need to be taken in order to achieve the best closure levels when doing using a decomposition method, and if there are other decomposition methods (e.g., wavelet transforms) that may be better. G10 and WBZ12-S performed better under SUN conditions when the radiation was less variable; under CLOUD conditions the increase in variability lowered their level of closure.

L12 had a systematic overestimation of G_0 producing a large degree of scatter in its closure though it achieved high daily closure levels both here and in Leuning et al. (2012). UFG and WBZ12-G performed consistently across the half-hour time-scales. Liebethal and Foken (2007) and Venegas et al. (2013) restricted UFG to daylight hours because the G_0/R_n ratio changes over the course of the day. In our study, overnight, UFG remained near-zero or positive when all the other methods became negative. WBZ12-G had high and relatively consistent levels of closure across the datasets. H09 did not show as well but this could be due to the time-step difference (Section 5.2) or/and the use of T_s (H09) compared to G_z (WBZ12-G).

Over longer averaging periods, the issue of intraday variability falls by the wayside and use of constant or diurnally-based values can produce high levels of closure (Leuning et al., 2012; Stoy et al., 2013; Anderson and Wang, 2014). Attempting closure at half-hour time-steps re-introduces the issue of variability in the diurnal cycle to the problem (Sun et al., 2013). The inability of some methods to capture variability in net radiation causes miss-estimations of the available energy even if the phasing matches. If not, closure at sub-daily timescales can suffer (e.g., H09) though it may not affect daily closure rates. Matching the phase does not imply good levels of closure at daily or sub-daily timescales even if the method can capture some of the daytime variability (e.g., UFG).

From the results and discussion above, recommendations as to the best methods can be made and are summarized in Table 5. Depending upon data availability, the recommended methods are CAL or WBZ12-G. Use of CAL or WBZ12-G makes using H09 and SM moot given their similarities. These methods were consistent across the different conditions and timescales whereas the other methods were more inconsistent across conditions or had larger offsets even with decent slopes.

Table 5
Recommended method based upon available data. No distinction is made for averaging timescale.

Data available	Available methods	Best choice(s)	Notes
T_s or G_z	WBZ12-G, WBZ12-S, H04, and G10	WBZ12-G	Need to calculate/measure thermal diffusivity
T_s, G_z, and T_z	Above and L12	WBZ12-G	Need all three variables
Above and R_n	Above and UFG	WBZ12-G	UFG only method that uses R_n in calculation
Above and VWC	CAL, SM, and H09	CAL and WBZ12-G	Assumes soil characteristics available; if not then only WBZ12-G

5. Conclusions

The performance of a method was dependent upon the variability in the diurnal radiation conditions and time step represented within the calculation. ALL represented the real-world-case and demonstrated the distinctions between the different method types. The sinusoid methods achieve good closure rates but their wave-based formulation limited their usefulness in trying to account for variation at shorter timescales. Using harmonic (Fourier) breakdown of the input parameters to account for variations was limited due to the time resolution of the data. The non-sinusoid methods were more consistent with their closure levels across the different subsets because they had minimal to no dependence upon diurnally-based inputs allowing them to adapt to changing conditions. Two main issues when calculating the soil heat flux were touched upon: phasing and data variability. Incorrect phasing can cause over/under-estimation of G_0 at the standard 30 min averaging period but at daily timescales phase mismatches can be moot. This is also true when for larger data sets that encompass a variety of conditions; the run to run phase variation will cancel through averaging. Regardless of timescale, capturing the variability and correct diurnal evolution is important. Given all of this, two methods were recommended as the preferred methods: CAL and WBZ12-G.

To close the energy balance at shorter time steps, the variability at the appropriate time scale needs to be represented within the G_0 calculation. Results from CLOUD showed that the increased variability over ALL can significantly decrease the levels of closure achieved by most methods at sub-daily timescales but had minimal effect at daily timescales. Under ALL-like conditions or at daily timescales, phasing and variability issues were resolved through

the averaging process so more methods could achieve better overall closure rates. But the longer averages start with short timescales so those influence can still be a factor.

Given the site specific nature of this type of work, the results presented here will apply to similar sites (dryer soils with sparse vegetation) but may not translate as well to wetter or more vegetated sites. The issues with the G_0 calculation are universal, but their degree of influence will differ depending upon soil wetness and shading of the measurement site. Similar work should be done at sites with different land-surface characteristics to see if similar recommendations and conclusions are reached.

Acknowledgments

We thank Qianyu Zhang, Shane Beard, and Tom Strong for help with the set-up, maintenance of the field site, and collection of data. Comments from two anonymous reviewers contributed to the improvement of this work. We acknowledge support by National Science Foundation AGS under Grant #1112938.

Appendix A. Equations for surface heat flux methodologies

A.1. Calorimetry (CAL)

CAL is the most common method to calculate G_0 (Gentine et al., 2012; Wang and Bou-Zeid, 2012). It has been used for surface heat flux calculations at numerous sites. Often it is the method to which other methods are compared in testing their effectiveness (Wang and Bou-Zeid, 2012). This method assumes that the soil heat flux plates are buried deep enough that they are protected from surface effects and calculates the heat stored in the overlying soil layer. G_0 is calculated from:

$$G_0 = G_z + C_v \frac{\partial T}{\partial t} \delta_z, \tag{A1}$$

where, G_0 is the surface soil heat flux, G_z is the measured heat flux at depth z, C_v is the volumetric soil heat capacity, $\frac{\partial T}{\partial t}$ is the change in the layer soil temperature with time, and δ_z is the change in depth from the surface to depth z. C_v can be calculated via:

$$C_v = \phi_s \rho_s c_s + \theta_{\delta_z} \rho_w c_w, \tag{A2}$$

where, ρ_s and ρ_w are the densities of the soil minerals and water respectively, c_s and c_w are the volumetric heat capacities of the soil minerals and water, respectively, θ_{δ_z} is the layer average volumetric water content, and ϕ_s is the soil mineral fraction. The heat capacity effects of air are neglected due to the much lower specific heat than either soil or water.

A.2. Gao et al., 2010 (G10)

G10 is derived based on the soil thermal conduction and convection (Gao et al., 2010). The version used here does not include the convection of heat due to the movement of water through the soil because the soil moisture was minimal at the site.

$$G(z,t) = \frac{\sqrt{2}\lambda A}{d} \exp\left(-z/d\right) \sin\left(wt - z/d + \frac{\pi}{4}\right), \tag{A3}$$

where, λ is the soil thermal conductivity, A is the amplitude of the surface diurnal temperature wave, w is the angular velocity of the earth ($2\pi/24$), d is the damping depth ($d = \sqrt{2k/w}$ where k is the soil thermal diffusivity), z is depth at which G is calculated, and t is time. The $\pi/4$ term is the phase lag of the sine wave due to the lag time between the surface heat flux and the measured in-soil heat flux. It is used to eliminate the hysteresis effect of the lag between the soil surface and the sub-surface measurements (Gao et al., 2010; Sun et al., 2013).

A.3. Heusinkveld et al., 2004 (H04)

Heusinkveld et al. (2004) incorporated the influence of the various frequencies on the soil heat flux and temperature waves via deconstructing the surface temperature through a Fourier series. G_0 is then reconstructed for each harmonic mode (n) through the highest mode (M) and is summed together for the contributions to G_0 from each harmonic mode to capture effects from multiple frequencies. The amplitude (A_n), phase (π_n), and radial frequency (w [$2\pi/N$; where N is the number of observations]) for each harmonic mode come from the Fourier transform (see Appendix A in Heusinkveld et al. (2004) for details). Again, $\pi/4$ is related to the phase lag with daily adjustments via π.

$$G_{z,t} = \sum_{n=1}^{M} \left[\begin{array}{c} A_n \frac{1}{k} (nwk)^{0.5} \exp^{-z\left(n(w/2000k)\right)^{0.5}} \\ * \sin\left(nwt + \varphi_n + \frac{\pi}{4} - z\left(n\frac{w}{2000k}\right)^{0.5} \right) \end{array} \right] \frac{\lambda}{10\pi} \tag{A4}$$

A.4. Leuning et al., 2012 (L12)

This method was put forth by Leuning et al. (2012). It requires less inputs and no *a priori* knowledge of soil thermal properties. Instead of calculating the heat storage flux in the soil layer between the heat flux plates and the surface, it calculates the damping depth based on the decay of the diurnal amplitude of the temperature wave ($\Delta T_{l,m}$) into the soil at depths z_l and z_m ($z_m > z_l$, positive downward) to un-damp the heat wave. The damping depth is calculated from:

$$z_D = \frac{z_m - z_l}{\ln\left(\Delta T_l / \Delta T_m\right)} \tag{A5}$$

The damping depth is then used to construct G_0 using the measured soil heat flux at z_m via:

$$G_0 = G_{z_m} \exp\left(z_m / z_d\right). \tag{A6}$$

Phase is adjusted outside Eq. A6 in that G_{z_m} trails G_0 by $\Delta t = 24 z_m/(2\pi z_d)$. The phase adjustment was specific to each day but the phase adjustment was always within a half hour from the mean phase change.

A.5. Wang and Bou-Zeid, 2012 Sinusoid method (WBZ12-S)

Wang and Bou-Zeid (2012) used G10 as a base to develop a more complex sinusoid method to include a second integral term and use the measured soil heat flux as the amplitude basis. This causes the depth term to be inverted so at the measured depth, z is equal to zero and at the surface z is equal to the measured depth. The integral term was defined as a "transient disturbance caused by starting the oscillation [...] from the initial condition which decays as t [time] increases." (Wang and Bou-Zeid, 2012). At the measurement depth, the integral term goes to zero and the expression collapses to being equivalent to G10 at their respective starting depths. ε is the phase variable and was used to match the phase with G10 and H04. Variables are the same as above with ξ being the integration variable:

$$G_z(t) = A \exp\left(-z\sqrt{w/2k}\right) \sin\left(wt + \varepsilon - z\sqrt{w/2k}\right) - \frac{2Ak}{\pi} \int_0^\infty \frac{\left[k\xi^2 \sin(\varepsilon) - w\cos(\varepsilon)\right] \xi \sin\left(\xi z\right)}{w^2 + k^2\xi^4} \exp\left(-k\xi^2 t\right) \mathrm{d}\xi \tag{A7}$$

A.6. Wang and Bou-Zeid, 2012 Green's function method (WBZ12-G)

This method is a Green's function-based derivation of the one-dimensional heat conduction equation as described in Wang and Bou-Zeid (2012). Like WBZ12-S, this method uses the measured soil heat flux as the base input. Wang (2012) does present a form of this method using soil temperature instead of soil heat flux; the form presented here uses the soil heat flux. Like WBZ12-S, z is determined relative to the depth of the soil heat flux plate so for surface calculation, z is equal to the depth of the heat flux plate. Wang and Bou-Zeid (2012) claim that the method is not limited by narrow boundary conditions found using Fourier series and only requires the soil thermal diffusivity whereas other methods, also require soil thermal conductivity. The discrete form of this method is:

$$G_0(n) = \frac{2G_z - J_{n-1}(G_0, \Delta F_z)}{\Delta F_z(1)} \tag{A8}$$

where, G_z is the soil heat flux at depth z. When calculating the soil heat flux via this formulation, z is equal to the depth of the buried heat flux plate, not the surface as in other methods. The other terms in this formulation are defined below, where t is time and erfc is the complimentary error function.

$$J_{n-1}(G_0, \Delta F_z) = G_{0_{(n-1)}} \Delta F_z(1) + \sum_{j=2}^{n-1} \left[G_{0_{(n-j+1)}} + G_{0_{(n-j)}} \right] \Delta F_z(j) \tag{A9}$$

$$F_z(j) = \mathrm{erfc}\left({}^{z}\!/\!\left(2\sqrt{kt_j}\right) \right). \tag{A10}$$

A.7. Hsieh et al., 2009 (H09)

This method is based on the half-order time derivative derived in Wang and Bras (1999) and used again in Hsieh et al. (2009). It is derived from the one-dimensional heat diffusion equation assuming a constant thermal diffusivity. Wang (2012) showed that WBZ12-G is mathematically equivalent to this method. The drawback for this method is that the integration time needs to start at a point where the heat flux is zero (i.e., requiring relatively uniform soil thermal conditions). Its advantage is that only one soil temperature measurement is required to calculate the heat flux though it must be at the same level as the desired heat flux (in this case, surface). It requires the volumetric heat capacity of the soil matrix meaning additional information regarding the local soil characteristics. Phase considerations are inherent into the method itself. In discrete form:

$$G(z,t) = 2\sqrt{\frac{kC_v}{\pi}} \sum_{i=0}^{N} \frac{T_{i+1} - T_i}{t_{i+1} - t_i} \left[\sqrt{t_N - t_{i+1}} - \sqrt{t_N - t_i} \right]. \tag{A11}$$

A.8. Universal function (UFG)

This method is an extension of using a percentage relationship between G_0 and R_n. The ratio between G_0 and R_n is not symmetric around solar noon and is dependent upon the density of the canopy over the surface and time of day (Santanello and Friedl, 2003; Liebethal and Foken, 2007). UFG attempts to account for the diurnal asymmetry by adjusting the ratio based on solar noon. A cosine function is used to make the diurnal wave whose amplitude is determined by the net radiation (R_n) and A and B are used to adjust the wave in relation to solar noon. The phase of the wave is determined by ΔT_s as well as the time of local solar noon (t, in seconds):

$$G_0(t) = A \cos\left(\frac{2\pi(t + 10800)}{B} \right) R_n, \tag{A12}$$

where,

$$A = 0.0074 \Delta T_s + 0.088 \tag{A13}$$

$$B = 1729 \Delta T_s + 65013 \tag{A14}$$

A.9. Simple measurement approach (SM)

SM uses in-situ measurements of soil heat flux and temperature to calculate the surface heat flux value (Liebethal and Foken, 2007). The method here is very similar to CAL in that it calculates the heat-storage component to be added to the measured heat flux. The difference from CAL is that CAL has one term that accounts for the change in time of the soil layer temperature while SM has two, one for the change in the surface temperature and one for the soil layer:

$$G_0(t) = G_z(t) + C_v z \left(\frac{T_s(t) - T_s(t - \Delta t) + 0.5\left[\Delta T(t - \Delta t) - \Delta T(t)\right]}{\Delta t} \right) \tag{A15}$$

where, z is the depth of the buried plate relative to the surface, Δt is the time step between measurements, and ΔT is the temperature difference between the surface and temperature at z (T_z) (Liebethal and Foken, 2007).

References

Anderson, R.G., Wang, D., 2014. Energy budget closure observed in paired eddy covariance towers with increased and continuous daily turbulence. Agric. For. Meteorol. 184, 204–209.

Campbell, G.S., Norman, J.M., 1998. An Introduction to Environmental Biophysics. Springer Science, New York.

Cava, D., Contini, D., Donateo, A., Martano, P., 2008. Analysis of short-term closure of the surface energy balance above short vegetation. Agric. For. Meteorol. 148, 82–93.

Foken, T., 2008. The energy balance closure problem: an overview. Ecol. Appl. 18, 1351–1367.

Foken, T., Aubinet, M., Finnigan, J.J., Leclerc, M.Y., Mauder, M., Paw, U.K.T., 2011. Results of a panel discussion about the energy balance closure correction for trace gases. Bull. Am. Meteorol. Soc. 92, ES13–ES18.

Gao, Z., Horton, R., Liu, H.P., 2010. Impact of wave phase difference between soil surface heat flux and soil surface temperature on soil surface energy balance closure. J. Geophys. Res. 115, D16112.

Gentine, P., Entekhabi, D., Heusinkveld, B., 2012. Systematic errors in ground heat flux estimation and their correction. Water Resour. Res. 48, W09541.

Heusinkveld, B.G., Jacobs, A.F.G., Holtslag, A.A.M., Berkowicz, S.M., 2004. Surface energy balance closure in an arid region: role of soil heat flux. Agric. For. Meteorol. 122, 21–37.

Hillel, D., San Diego,2004. Introduction to Environmental Soil Physics. Elsevier Academic Press, San Diego.

Higgins, C.W., 2012. A-posteriori analysis of surface energy budget closure to determine missed energy pathways. Geophy. Res. Lett. 39, L19403.

Hsieh, C.-I., Huang, C.-W., Kiely, G., 2009. Long-term estimation of soil heat flux by single layer soil temperature. Int. J. Biometeorol. 53, 113–123.

Jacobs, A.F.G., Heusinkveld, B.G., Holtslag, A.A.M., 2008. Toward closing the surface energy budget of a mid-latitude grassland. Boundary-Layer Meteorol. 126, 125–136.

Kohsiek, W., Liebethal, C., Foken, T., Vogt, R., Oncley, S.P., Bernhofer, C.H., Debruin, H.A.R., 2007. The energy balance experiment EBEX-2000, Part III: behaviour and quality of the radiation measurements. Boundary-Layer Meteorol. 123, 55–75.

Kustas, W.P., Prueger, J.H., Hatfield, J.L., Ramalingam, K., Hipps, L.E., 2000. Variability in soil heat flux from a mesquite dune site. Agric. For. Meteorol. 103, 249–264.

Leuning, R., van Gorsel, E., Massman, W.J., Isaac, P.R., 2012. Reflections on the surface energy imbalance problem. Agric. For. Meteorol. 156, 65–74.

Li, Y., Liu, S., Wang, S., Miao, Y., Chen, B., 2014. Comparative study on methods for computing soil heat storage and energy balance in arid and semi-arid areas. J. Meteorol. Res. 28, 308–322.

Liebethal, C., Foken, T., 2007. Evaluation of six parameterization approaches for the ground heat flux. Theor. Appl. Climatol. 88, 43–56.

Liebethal, C., Huwe, B., Foken, T., 2005. Sensitivity analysis for two ground heat flux calculation approaches. Agric. For. Meteorol. 132, 253–262.
Mayocchi, C.L., Bristow, K.L., 1995. Soil surface heat flux: some general questions and comments on measurements. Agric. For. Meteorol. 75, 43–50.
Mauder, M., Foken, T., 2006. Impact of post-field data processing on eddy covariance flux estimates and energy balance closure. Meteorol. Z. 15, 597–609.
Mauder, M., Oncley, S.P., Vogt, R., Weidinger, T., Ribeiro, L., Bernhofer, C., Foken, T., Kohsiek, W., De Bruin, H.A.R., Liu, H., 2007. The energy balance experiment EBEX-2000, Part II: intercomparison of eddy-covariance sensors and post-field processing methods. Boundary-Layer Meteorol. 123, 29–54.
Núnez, C.M., Varas, E.A., Meza, F.J., 2010. Modelling soil heat flux. Theor. Appl. Climatol. 100, 251–260.
Ochsner, T.E., Sauer, T.J., Horton, R., 2007. Soil heat storage measurements in energy balance studies. Agron. J. 99, 311–319.
Oncley, S.P., Foken, T., Vogt, R., Kohsiek, W., DeBruin, H.A.R., Bernhofer, C., Christen, A., van Gorsel, E., Grantz, D., Feigenwinter, C., Lehner, I., Liebethal, C., Liu, H., Mauder, M., Pitacco, A., Ribeiro, L., Weidinger, T., 2007. The energy balance experiment EBEX-2000, Part I: overview and energy balance. Boundary-Layer Meteorol. 123, 1–28.
Santanello, J.A., Friedl, M.A., 2003. Diurnal covariation in soil heat flux and net radiation. J. Appl. Meteorol. 42, 851–862.
Schotanus, P., Nieuwstadt, F.T.M., De Bruin, H.A.R., 1983. Temperature measurement with a sonic anemometer and its application to heat and moisture flux. Boundary-Layer Meteorol. 26, 81–93.
Stoy, P.C., Mauder, M., Foken, T., et al., 2013. A data-driven analysis of energy balance closure across FLUXNET research sites: the role of landscape scale heterogeneity. Agric. For. Meteorol. 171–172, 137–152.
Sun, T., Wang, Z.-H., Ni, G.-H., 2013. Revisiting the hysteresis effect in surface energy budgets. Geophys. Res. Lett. 40, 1741–1747.
Venegas, P., Gradón, A., Jara, J., Paredes, J., 2013. Hourly estimation of soil heat flux density at the soil surface with three models and two field methods. Theor. Appl. Climatol. 112, 45–59.
Vickers, D., Mahrt, L., 1997. Quality control and flux sampling problems for tower and aircraft data. J. Atmos. Ocean. Technol. 14, 512–526.
Wang, Z.-H., 2012. Reconstruction of soil thermal field from a single depth measurement. J. Hydrol. 464–465, 541–549.
Wang, Z.-H., Bou-Zeid, E., 2012. A novel approach for the estimation of soil ground heat flux. Agric. For. Meteorol. 154–155, 214–221.
Wang, J., Bras, R.L., 1999. Ground heat flux estimated from surface soil temperature. J. Hydrol. 216, 214–226.
Webb, E.K., Pearman, G.L., Leuning, R., 1980. Correction of flux measurements for density effects due to heat and water vapour transfer. Q. J. R. Meteorol. Soc. 106, 85–100.
Wilczak, J.M., Oncley, S.P., Stage, S.A., 2001. Sonic anemometer tilt correction algorithms. Boundary-Layer Meteorol. 99, 127–150.
Wilson, K., Goldstein, A., Falge, E., Aubinet, M., Baldocchi, D., Berbigier, P., Bernhofer, C., Ceulemans, R., Dolman, H., Field, C., Grelle, A., Ibrom, A., Law, B.E., Kowalski, A., Meyers, T., Moncrieff, J., Monson, R., Oechel, W., Tenhunen, J., Valentini, R., Verma, S., 2002. Energy balance closure at FLUXNET sites. Agric. For. Meteorol. 113, 223–243.
Wohlfahrt, G., Widmoser, P., 2013. Can an energy balance model provide additional constraints on how to close the energy imbalance? Agric. For. Meteorol. 169, 85–91.
Yang, K., Wang, J., 2008. A temperature prediction-correction method for estimating soil heat flux from soil temperature and moisture data. Sci. China Ser. D: Earth Sci. 51, 721–729.